Two-eigenfunction correlation in a multifractal metal and insulator

E. Cuevas
Departamento de Física, Universidad de Murcia, E30071 Murcia, Spain

V. E. Kravtsov
The Abdus Salam International Centre for Theoretical Physics, P.O. Box 586, 34100 Trieste, Italy
and Landau Institute for Theoretical Physics, 2 Kosygina Street, 117940 Moscow, Russia
(Received 9 August 2007; published 19 December 2007)

We consider the correlation of two single-particle probability densities $|\Psi_E(\mathbf{r})|^2$ at coinciding points $\mathbf{r}$ as a function of the energy separation $\omega=|E-E'|$ for disordered tight-binding lattice models (the Anderson models) and certain random-matrix ensembles. We focus on the parameter range close to but not exactly at the Anderson localization transition. We show that even away from the critical point, the eigenfunction statistics exhibit the remnant of multifractality characteristic of the critical states. By a combination of numerical results on the Anderson model and analytical and numerical results for the relevant random-matrix theories, we identified the Gaussian random-matrix ensembles that describe the multifractal features both in the metal and in the insulator phases. This analysis reveals other features of the structure of eigenfunctions: (i) eigenfunction mutual avoidance at large energy separations, (ii) competition between repulsion of centers of localization and enhanced overlap by tails at small energy separations, and (iii) possible existence of a different metallic phase in higher dimensions.

DOI: 10.1103/PhysRevB.76.235119 PACS number(s): 72.15.Rn, 72.70.+m, 72.20.Ht, 73.23.−b

I. INTRODUCTION

Eigenfunction and spectral statistics in quantum systems with quenched disorder were a subject of intense study[1] in the context of mesoscopic fluctuations of conductance and density of states (DOS), in particular, in quantum dots.[2] For this application, the most relevant is the regime of weak deviation[3,4] from the Wigner-Dyson statistics given by the conventional random-matrix theory (RMT).[5] Disordered multichannel quantum wires are the most important example of systems where single-particle eigenstates are all localized. Here, the statistics of eigenstates require a nonperturbative treatment using the formalism of nonlinear sigma model[6] or banded random matrices.[7] A special class is systems with the critical, multifractal (MF) eigenstate statistics.[1,8,9] Two-dimensional disordered metals fall into this class[10] provided that effects of localization are suppressed by magnetic field. Otherwise, one can speak only on weak multifractality, which turns to localization before being fully developed. The true physical realizations of the critical, MF eigenstate statistics are systems at the critical point of the Anderson localization transition[11,12] and the integer quantum Hall systems at the center of the Landau band.[13] Importantly, the class of systems with MF eigenstate statistics also allows for a random-matrix representation,[8] in particular, using the power-law banded random matrices (PLBRMs).[14]

Another field of intense research is the interplay between disorder and electron interaction with the seminal results on quantum correction to the tunnel DOS and conductivity[15] of disordered two-dimensional metals and the correction to superconducting transition temperature due to a simultaneous effect of disorder and the Coulomb interaction.[16] In all those works, disorder and interaction are taken into account essentially perturbatively along the lines given in Ref. 17. Recently, there was an attempt[18] to consider the problem of superconductivity near the Anderson transition, in which disorder has been treated nonperturbatively by *postulating* the MF statistics of one-particle states $\Psi_i(\mathbf{r})$ that enter the matrix element of a phenomenological electron attraction:

$$J_{ij} = g \int d\mathbf{r} \Psi_i(\mathbf{r})^2 \Psi_j(\mathbf{r})^2. \tag{1}$$

In particular, the simplest quantity of interest is the disorder average matrix element $\langle J_{ij} \rangle$ at a given energy separation ω between one-particle energies E_i and E_j. For real eigenfunctions (orthogonal symmetry class), it is proportional to the correlation function $C(\omega)=K(\omega)/R(\omega)$, where

$$K(\omega) = \int d\mathbf{r} \sum_{i,j} \langle |\Psi_i(\mathbf{r})|^2 |\Psi_j(\mathbf{r})|^2 \delta(E_i - E_j - \omega) \rangle, \tag{2}$$

and $R(\omega)=\Sigma_{ij}\langle \delta(E_i-E_j-\omega)\rangle$ is the spectral correlation function which is close to 1 for ω much greater than the mean level spacing. The correlation function $C(\omega)\approx K(\omega)$ is the main subject of the present paper.

The correlation function defined by Eq. (2) is a measure of overlap of *two different* eigenfunctions. For truly extended normalized states (e.g., in a quantum dot), $|\Psi_i(\mathbf{r})|^2=1/\mathcal{V}$ and, thus, $C(\omega)\mathcal{V}=1$, where $\mathcal{V}$ is a system volume. Remarkably, $C(\omega)\mathcal{V}=1$ is also valid for the best studied example of localized states in a quantum disordered wire. In this case, two states are typically not overlapping, but with a small probability of $\xi^d/\mathcal{V}$ (where ξ is the localization radius) they are localized in the same place, and then the integral in Eq. (2) is of the order of the inverse localization volume $1/\xi^d$.

There are cases, however, when an eigenfunction $\Psi_i(\mathbf{r})$ does not occupy all the available volume or all the localization volume, and the typical amplitude $|\Psi_i(\mathbf{r})|^2$ is not just the inverse volume (for extended states) or the inverse localization volume (for localized states). In this case, a nontrivial

behavior of the correlation function $C(\omega)$ is expected. Such a situation is realized near the critical point of the Anderson localization transition. In the vicinity of this point in the region of extended states (*multifractal metal*) or in the region of localized states (*multifractal insulator*), the system retains the characteristic features of the critical multifractal statistics of eigenstates, which makes it qualitatively different from both a normal metal or a normal Anderson insulator.

In this paper, we will identify and quantify such characteristic features in the correlation function $C(\omega)$ and give their interpretation in terms of the typical behavior of single-particle states. To attain this goal, we will combine analytical results for the PLBRM with numerics on the PLBRM and the Anderson model. We especially focus on the dependence of $C(\omega)$ on the energy difference ω in the crossover region in the vicinity of but not exactly at the Anderson transition point, which has not been studied so far.

The paper is organized as follows. In Sec. II, we give a brief introduction into the subject of multifractality of critical eigenstates, focusing on the main effect of multifractality which is the critical enhancement of eigenfunction correlations. In Sec. III, we give a cartoon of the off-critical states in a multifractal metal and a multifractal insulator, and introduce the random-matrix theories which may describe them. In Sec. IV, we present the results of an analytical theory of eigenfunction correlations for a class of almost diagonal Gaussian random matrices, which all the RMTs suggested to describe strong multifractality fall into. In Sec. V, we consider the two-eigenfunction correlation function exactly at the critical point of the localization transition in the three-dimensional (3D) Anderson model and for the critical random-matrix ensemble in the limit of strong multifractality. We show that the dynamical scaling relationship suggested by Chalker is not violated even in the limit when the fractal dimensions are very small. In Sec. VI, we describe the phenomenon of eigenfunction mutual avoidance, and present a qualitative picture that simultaneously explains the enhancement of eigenfunction correlations at small energy separations and the eigenfunction mutual avoidance at large energy separations. In Sec. VII, we consider the properties of eigenfunction correlations in a multifractal insulator. In particular, we describe the phenomenon of logarithmic enhancement of eigenfunction correlations at small energy separations in the two-dimensional (2D) and 3D Anderson insulators and show the absence of such enhancement in the quasi-one-dimensional (quasi-1D) case. We also suggest a truncated critical random-matrix (RM) ensemble that describes all the principal features of eigenfunction correlations in the 3D multifractal insulator. Section VIII is devoted to the random-matrix description of the multifractal metal. We show that the subcritical PLBRM suggested in Ref. 14 gives a reasonable agreement with the 3D Anderson model. By an analytical treatment of this RM model, we found the region of parameters where the eigenfunction correlations become effectively short range in the energy space, which may point to the existence of a different metal phase above some critical dimensionality in the multidimensional Anderson model. In Sec. IX, we list all the principal results of this paper.

II. MULTIFRACTALITY OF CRITICAL EIGENFUNCTIONS

The "standard" model (the Anderson model) for the Anderson localization transition in $d>2$ dimensions is the tight-binding model with the hopping constant $V=1$ and random on-site energies ε_i characterized by the distribution function $\mathcal{P}(\varepsilon_i)$, which is frequently chosen constant $\mathcal{P}(\varepsilon_i)=1/W$ in the interval $[-W/2, W/2]$ and zero otherwise. There is a vast literature (see, e.g., Ref. 19 and references therein) on the numerical investigation of the Anderson localization transition in this model on a 3D lattice. Recently, also higher dimensions $d>3$ have become accessible to modern computers.[20] While the earlier studies of this model were focused on the critical behavior of the localization and/or correlation length ξ near the critical disorder W_c, the recent works were mostly related to the statistics of critical eigenfunctions. The multifractality of critical eigenfunctions predicted in Ref. 11 almost immediately after the emergence of the scaling theory of localization has been confirmed and quantified in detail.

The results obtained for the Anderson model exactly at the critical point seem to be very well described[21] by the critical PLBRM model.[8,14] This model is defined as an ensemble of random Hermitian matrices, the entries H_{ij} of which fluctuate independently around zero with the variance

$$\langle |H_{ij}|^2 \rangle = \begin{cases} \beta^{-1}, & i=j \\ \dfrac{1}{2\left[1+\dfrac{|i-j|^2}{b^2}\right]}, & i \neq j, \end{cases} \tag{3}$$

where $\beta=1$, 2, and 4 for the Dyson orthogonal, unitary, and symplectic symmetry classes,[5] and b is the parameter that controls the multifractality exponents. The solutions $\vec{\Psi}_n = \{\Psi_n(1), \ldots, \Psi_n(N)\}$ of the Schrödinger equation

$$\sum_{r'} H_{rr'} \Psi_n(r') = E_n \Psi_n(r)$$

can be considered as being defined on a one-dimensional lattice $r \in \{1, \ldots, N\}$, where the tight-binding Hamiltonian (with possible long-range hops) $H_{rr'}$ is operating.

This model has been studied and its comparison with the Anderson model in d dimensions has been done predominantly for the statistical moments P_n of a *single* eigenstate at a given energy E:

$$P_q(E) = \rho^{-1} \sum_n \sum_{\mathbf{r}} \langle |\Psi_n(\mathbf{r})|^{2q} \delta(E-E_n) \rangle. \tag{4}$$

The best known example is the inverse participation ratio (IPR) given by the second moment P_2. The multifractal statistics of a single eigenstate is characterized by the moment P_q that scales with the system volume $\mathcal{V}$ or the total number of sites N as

$$P_q \propto N^{-(q-1)d_q/d}, \tag{5}$$

where $d_q<d$ is the fractal dimension corresponding to the qth moment. The existence of the scaling law Eq. (5) and the dependence of the exponent d_q on q are the principal features of *eigenfunction multifractality*. The fractal exponents d_q de-

pend also on the symmetry class β and the space dimensionality d. For the critical PLBRM Eq. (3), the dependence on d is modeled by the dependence of d_q on the parameter b.

The critical scaling Eq. (5) with respect to the system size N has its *dynamical* counterpart when, instead of one single eigenfunction, one considers the correlation function Eq. (2) of *two* eigenfunctions at an energy separation $\omega=|E-E'|$ between them. This scaling has been suggested by Chalker[12,13] many years ago:

$$C(\omega) = \frac{1}{N}\left(\frac{E_0}{\omega}\right)^{\mu}, \quad \delta < \omega < E_0, \tag{6}$$

where

$$\mu = 1 - \frac{d_2}{d}, \tag{7}$$

δ is the mean level spacing, and E_0 is the upper cutoff of multifractality. Numerics on the integer quantum Hall systems and in the critical point of the 3D Anderson model was consistent[22,23] with this scaling.

An important feature of Eq. (6) is that the exponent μ in the ω dependence is smaller than 1. Even in the limit of infinitely small correlation dimension d_2, the correlation function decays slowly as $1/\omega$. This implies that the sparse critical states separated by a large energy distance are still well overlapping,[24] in contrast to strongly localized states which typically do not overlap even for nearest neighbors in the energy space. The reason for such a behavior and the physical meaning of the energy scale E_0 will be discussed in Sec. VI.

As the correlation function is equal to $C(\omega) \approx 1/N$ both for the truly extended and the ideal localized states, Eq. (6) implies the *critical enhancement* of eigenfunction correlations for $\omega < E_0$. This enhancement of *single-particle* density correlations leads to an enhancement of matrix elements of *two-body* local interactions. It is crucially important, e.g., for electron interaction near the Anderson localization transition, in particular, for the superconducting transition temperature.[18] To illustrate this point, we present in Fig. 1 the results of numerical diagonalization of the critical PLBRM, the classical Wigner-Dyson RM $\langle|H_{ij}|^2\rangle$=const with extended eigenstates, and the ensemble of conventional banded random matrices[7] with exponentially decreasing entries $\langle|H_{ij}|^2\rangle \propto \exp(-|i-j|/B)$, which describes strongly localized eigenstates in quasi-1D disordered systems. The critical enhancement of eigenfunction correlations is evident from this plot.

The physical origin of the enhancement is twofold: (i) a critical eigenfunction "occupies" only part of the available space which by normalization $\Sigma_r|\Psi(\mathbf{r})|^2=1$ enhances its amplitude, and (ii) the supports (the manifold of $\{\mathbf{r}\}$, where $|\Psi(\mathbf{r})|^2$ is essentially nonzero) of different critical eigenfunctions are strongly overlapping. It is important that both conditions are fulfilled simultaneously. For instance, condition (i) is fulfilled for localized states even better than for the critical ones, but the lack of condition (ii) levels off the gain in the correlation function $C(\omega)$. On the contrary, in a metal, condition (ii) is trivially fulfilled, but the eigenfunction amplitude is small.

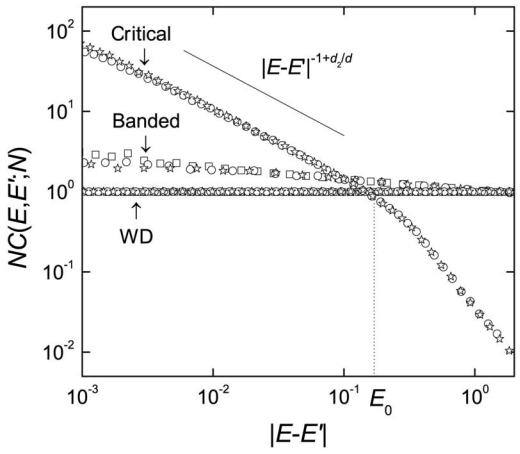

FIG. 1. Critical enhancement of eigenfunction correlation. Results of exact diagonalization of the critical PLBRM at $b=0.1$, the banded random matrices with $B=5$, and Wigner-Dyson RM are represented by squares ($N=200$), circles ($N=1000$), and stars ($N=2000$).

III. OFF-CRITICAL STATES AND THEIR RANDOM-MATRIX REPRESENTATIONS

Gaussian random-matrix models proved to be an efficient and universal theoretical tool for describing complex systems. The success was partially due to the available analytical solutions[5,7] and partially due to efficient algorithms of numerical diagonalization of matrices. Therefore, it is highly desirable to have random-matrix models that describe not only the critical MF eigenstates, but also localized and extended eigenstates in the *vicinity* of the Anderson transition. The criterion to select such models is a qualitative and (when possible) a quantitative agreement with the results on the 3D Anderson model.

As will be demonstrated below, the correlation function $C(\omega)$ in the 3D Anderson model contains the critical power-law behavior Eq. (6) well beyond the Anderson transition point. As a matter of fact, the correlation function $C(\omega)$ is indistinguishable from the critical one until the dynamic length $L_\omega = 1/(\rho\omega)^{1/d}$ (ρ is the mean DOS) exceeds the localization and/or correlation length ξ. For $L_\omega > \xi$, or ω smaller than the level spacing in the localized volume $\delta_\xi \sim 1/\rho\xi^d$, the correlation function loses its critical features and shows typical features of a metal or an isulator.

This allows us to suggest the following cartoon of typical eigenfunctions in the vicinity of the localization transition shown in Fig. 2. Namely, a typical localized state in a multifractal insulator can be viewed as a "piece of multifractal" of the size of the localization radius ξ [Fig. 2(b)]. in contrast to a conventional localized state where all the localization volume is more or less homogeneously "filled" [Fig. 2(a)]. In the same way, typical extended states on the metallic side of the localization transition (multifractal metal) should look like a mosaic made of such "pieces of multifractal" [Fig. 2(c)].

Based on the persistence of the critical behavior beyond the critical region, it is natural to assume that the random-matrix model for the extended states near the critical point

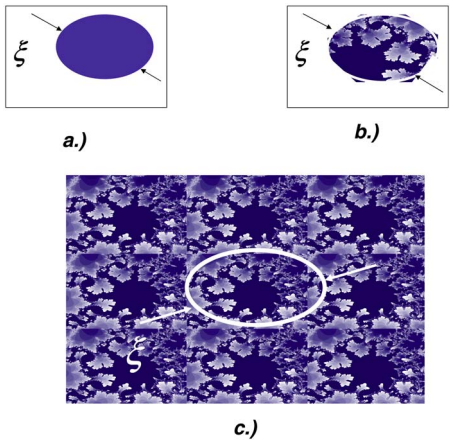

FIG. 2. (Color online) 2D cartoon of (a) conventional localized state, (b) localized state in a multifractal insulator, and (c) extended state in a multifractal metal. The darker regions correspond to higher eigenfunction amplitude. The localization and/or correlation radius ξ is shown in each case.

and the localized states on the other side of the transition should bear features of the critical RMT.

Let us start by constructing a random-matrix model for the multifractal insulator. Given that the quasi-1D insulator is well described by the banded random matrices[7] with exponentially decaying variance $\langle|H_{ij}|^2\rangle=\exp\{-|i-j|/B\}$, we suggest the following hybrid RM model as a model for the multifractal insulator:

$$\langle|H_{ij}|^2\rangle=\begin{cases}\beta^{-1}, & i=j\\ \dfrac{b^2}{2(|i-j|^2+b^2)}\exp\left\{-\left(\dfrac{|i-j|}{B}\right)^{\eta}\right\}, & i\neq j.\end{cases} \tag{8}$$

As compared with the critical PLBRM model Eq. (3), the model Eq. (8) contains an additional parameter B which sets in a finite localization radius $\xi(B)$. It also contains an exponent η which depends on the space dimensionality d of the disordered lattice model we would like to model by the RMT. In Sec. VIII, we give both analytical and numerical arguments in favor of the choice

$$\eta=1/d.$$

Another candidate has been suggested in Ref. 14:

$$\langle|H_{ij}|^2\rangle=\begin{cases}\beta^{-1}, & i=j\\ \dfrac{1}{2\left[1+\left(\dfrac{|i-j|}{b}\right)^{2\alpha}\right]}, & i\neq j.\end{cases} \tag{9}$$

In this case, the localization radius ξ is controlled by the variable exponent α of the power law. For a multifractal insulator, $\alpha>1$.

The possible RM models for a multifractal metal are also constructed as deformations of the critical PLBRM. The model Eq. (9) for $\alpha<1$ is believed[14] to describe the multifractal metal. One can also think that the Gaussian RMT

$$\langle|H_{ij}|^2\rangle=\begin{cases}\beta^{-1}, & i=j\\ \dfrac{1}{2\left[1+\dfrac{|i-j|^2}{b^2}\right]}+\left(\dfrac{b}{B}\right)^2, & i\neq j,\end{cases} \tag{10}$$

which is a hybrid of the critical PLBRM and the Wigner-Dyson RMT, is also suitable for this purpose. Below, we will study all those RM models in detail and compare the corresponding results for the correlation function $C(\omega)$ with the results obtained by numerical diagonalization of the d-dimensional Anderson model.

IV. ALMOST DIAGONAL GAUSSIAN RANDOM-MATRIX THEORY: ANALYTICAL RESULTS FOR $C(\omega)$

The characteristic properties of multifractal statistics of critical and off-critical states are best seen when the multifractality is strong. This is the case where the parameter $b\ll 1$ in Eqs. (3) and (8)–(10) is small. On the other hand, this is exactly the limit where the typical off-diagonal elements of H_{ij} are small compared to diagonal ones. Such matrices [referred to as *almost diagonal* random matrices (ADRMs)] may possess a nontrivial statistics of eigenfunctions which justifies their special study.[25,27] The idea of the analytical treatment of ADRM, first suggested in Ref. 26 and used in Ref. 21 to compute the correlation dimension d_2 for the critical PLBRM model Eq. (3), is similar to the virial expansion in dilute gases. However, instead of taking into account two-, three-, and multiple-particle collisions, one considers a progressively increasing number of interacting resonance sites coupled by a small off-diagonal matrix element H_{ij}. Recently, the virial coefficients for the Gaussian ADRM with an arbitrary (but small) variance $\sigma^2(|i-j|)=2\langle|H_{ij}|^2\rangle$ were expressed through the supersymmetric field theory,[27] and the correlation function $C(\omega)$ has been explicitly calculated in the two-state approximation for the *unitary* symmetry class $\beta=2$. The result is the following:

$$C(\omega)=\frac{k(\omega)}{Nr(\omega)}, \tag{11}$$

where

$$k(\omega)=\sum_{n=1}^{N}\left[\left(2\bar{\omega}+\frac{1}{\bar{\omega}}\right)e^{-\bar{\omega}^2}\frac{\sqrt{\pi}}{2}\,\mathrm{Erfi}(\bar{\omega})-1\right] \tag{12}$$

and

$$r(\omega)=\frac{\sqrt{\pi}}{N}\sum_{n=1}^{N}\bar{\omega}e^{-\bar{\omega}^2}\,\mathrm{Erfi}(\bar{\omega}). \tag{13}$$

In Eqs. (12) and (13), we denote

$$\bar{\omega}=\frac{\omega}{\sqrt{2\sigma^2(n)}}=\frac{\omega}{2\sqrt{\langle|H_{i,i+n}|^2\rangle}} \tag{14}$$

and $\mathrm{Erfi}(z)=\frac{2}{\sqrt{\pi}}\int_0^z e^{t^2}dt$.

The result given by Eqs. (12) and (13) is valid in the limit when

$$\sum_{n=1}^{N} \sigma(n) \ll \sqrt{\langle |H_{ii}|^2 \rangle}. \quad (15)$$

For the RMT defined by Eqs. (8) and (9) with $\alpha > 1$, which are suggested to describe the multifractal insulator, the sum over n in Eq. (15) converges. Then the validity of Eqs. (12) and (13) is independent of the matrix size N in the limit $N \to \infty$ and is controlled only by a small parameter $b \ll 1$. On the contrary, for the models of the multifractal metal described by Eqs. (10) and (9) with $\alpha < 1$, the sum in Eq. (15) diverges at large N. Then Eqs. (12) and (13) are only valid for $N < \xi$, where we define the *correlation radius* ξ as follows:

$$\sum_{n=1}^{\xi} \sigma(n) = \sqrt{\langle |H_{ii}|^2 \rangle}. \quad (16)$$

We will show below that a good qualitative description of the metal phase in the limit $N \to \infty$ can still be obtained from the above theory if one substitutes ξ for N in Eqs. (12) and (13).

Equations (12)–(16) will be used throughout the paper to analyze different random-matrix ensembles suggested as possible models for critical eigenstates and off-critical states in multifractal metal and insulator.

V. TWO-EIGENFUNCTION CORRELATIONS AT CRITICALITY

It is not *a priori* clear that the critical power-law behavior Eq. (6) and the dynamical scaling relationship Eq. (7) hold true for all systems where Eq. (5) is valid. In particular, it is interesting to study the correlation function Eq. (2) in the limit of strong multifractality when $d_2 \to 0$. Below, we will derive an *analytical* formula for the critical PLBRM in the limit $b \to 0$, which corresponds[20] to $d_2 \to 0$, and confirm the scaling law Eq. (7) by numerical diagonalization of PLBRM with very small b.

One can easily see from Eqs. (12)–(14), in which we plug in Eq. (3), that in the interval $\frac{b}{N} \ll |E - E'| \ll b$ the correlation function $C(\omega)$ given by these equations has an asymptotic power-law behavior Eq. (6) with $\mu = 1$:

$$NC(\omega) = \frac{E_0}{|\omega|}, \quad E_0 = \left(\frac{\pi}{2}\right)^{3/2} b. \quad (17)$$

Applying Eq. (15) to the critical PLBRM Eq. (3) gives the criterion of validity $\ln N \ll 1/b \sim 1/d_2$, in which case one cannot distinguish between N^{1-d_2} and N, or, correspondingly, between ω^{-1+d_2} and $1/\omega$. Thus, the analytical formulas Eqs. (12) and (3) are consistent with the scaling relationship Eq. (7), given that $d_2(b) \to 0$ as $b \to 0$.

A comparison of the analytical results and the results of numerical diagonalization of the critical PLBRM with $\beta = 2$ and $b = 0.06$ is shown in Fig. 3. The coincidence is very good for large energy separations. The deviation at small energy separations is due to the difference in the values of μ. The exponent $\mu = 1$ for the analytical curve and $\mu = 0.86$ for the numerical curve, which is very close to the prediction of Eq. (7), $\mu = 1 - d_2 \approx 0.865$, where d_2 is found from the numerical data for $P_2(N)$ and Eq. (5).

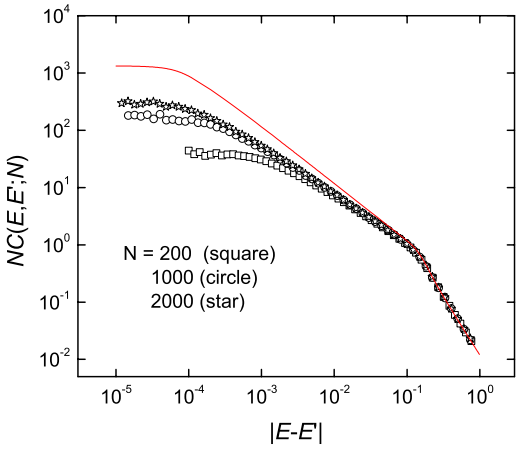

FIG. 3. (Color online) Two-eigenfunction correlation function $C(\omega)$ for the critical PLBRM with $\beta = 2$, $b = 0.06$, and $N = 200$ (squares), 1000 (circles), and 2000 (stars). The analytical curve at $N = 2000$ given by Eqs. (11)–(13) is shown by a solid line.

The scaling relationship Eq. (7) is further checked in Fig. 4, where the numerical data for μ and $1 - d_2$ are plotted as a function of b. The fulfillment of this relationship down to b as small as 0.005 and an agreement with the theoretical prediction of Ref. 21 are spectacular. Thus, from the combination of analytical and numerical results, we conclude that the Chalker scaling Eqs. (6) and (7) is valid for arbitrary small b and, thus, for arbitrary strong multifractality.

Finally, we demonstrate how well the critical PLBRM Eq. (3) describes the two-eigenfunction correlations in the 3D Anderson model at the mobility edge. To this end we modify the distribution of the on-site energies in the Anderson model from the standard rectangular box distribution to the triangular distribution where the mobility edge corresponds to $E_c = \pm 3.5$. The correlation function $C(\omega)$ with E, E' near the mobility edge is shown in Fig. 5. It coincides almost exactly with the corresponding curve resulting from numerical diagonalization of the critical PLBRM ensemble with only one fitting parameter $b = 0.42$.

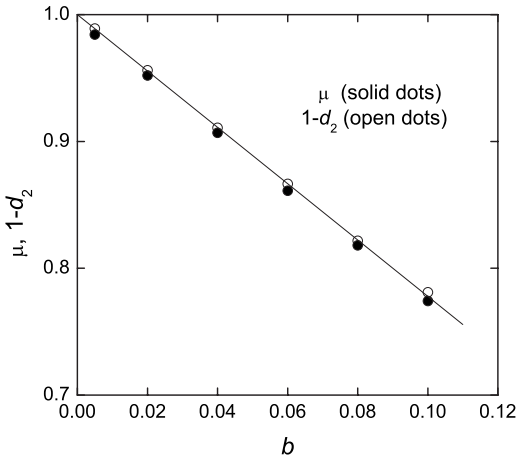

FIG. 4. The scaling relationship between μ and d_2 for the $\beta = 2$ critical PLBRM. The solid line is the prediction based on Ref. 21, $d_2 = \frac{\pi}{\sqrt{2}} b$.

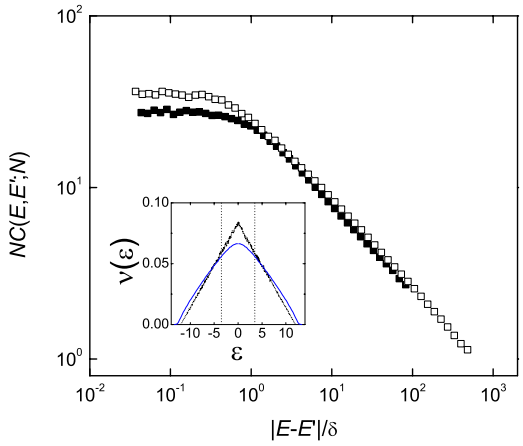

FIG. 5. (Color online) Two-eigenfunction correlation function for the 3D Anderson model (orthogonal symmetry class) with a triangular distribution of random on-site energies (solid symbols) and the critical PLBRM Eq. (3) with $\beta=1$ and $b=0.42$ (open symbols). The energy difference $\omega=|E-E'|$ is measured in units of mean level spacing. The inset shows the mean density of states; the mobility edge corresponds to $\varepsilon=\pm 3.5$. The energies E,E' were taken from the window (3.3, 3.7) for the 3D Anderson model and from $(-0.2,0.2)$ for the critical PLBRM. The slope of the critical power law Eq. (6) is 0.52 in both cases, which corresponds to $d_2/d=0.48$.

VI. EIGENFUNCTION MUTUAL AVOIDANCE AND STRATIFICATION OF COORDINATE SPACE

Results of both numerical and analytical calculations presented in Fig. 3 reveal another unexpected feature of eigenfunction correlation which appears to be common to all ADRMs. Surprisingly, it is also present for the 3D Anderson model both in the metal phase and in the insulator phase (see Fig. 6). This is the *negative* eigenfuncton correlations for $\omega=|E-E'|>E_0\sim b$. Indeed, one can see from Figs. 3 and 6

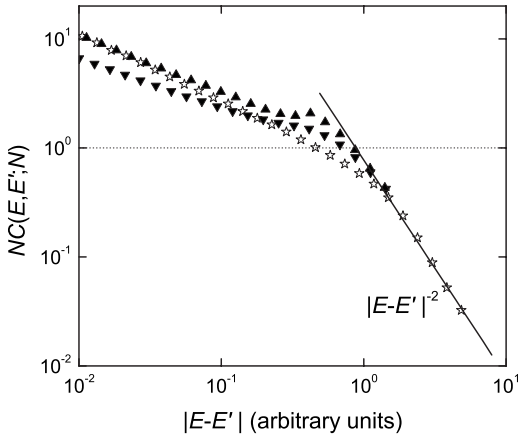

FIG. 6. Eigenfunction mutual avoidance for the PLBRM with $b=0.42$ (stars) and 3D Anderson insulator (up triangles) and metal (down triangles). The dotted line corresponds to the limit of uncorrelated eigenfunctions; the solid line corresponds to the power law $1/\omega^2$. Points below the dotted line correspond to eigenfunction mutual avoidance.

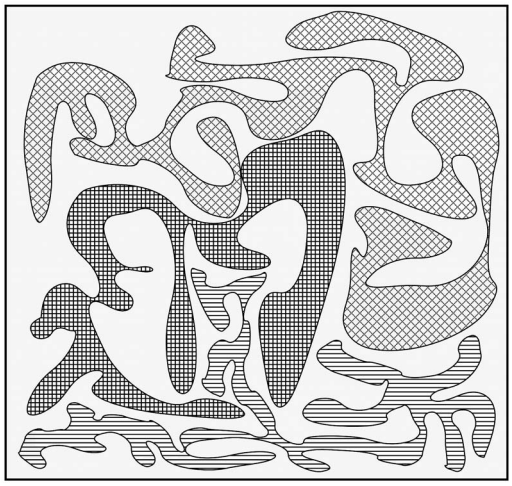

FIG. 7. A cartoon of stratification of the coordinate space: different nonintersecting supports shown by different textures. Each support corresponds to a shell of states occupying this support and, thus, are strongly overlapping; states belonging to different shells do not overlap. The stratification of space explains both strong correlations of states at energy separation ω smaller than the single-shell bandwidth E_0 and mutual avoidance of eigenstates for $\omega>E_0$.

that for large enough ω, the correlation function $C(\omega)$ goes below the uncorrelated limit $C(\omega)=1/N$, which corresponds to $\langle|\Psi_i|^2|\Psi_j|^2\rangle=\langle|\Psi_i|^2\rangle\langle|\Psi_j|^2\rangle=1/N^2$. We denote by E_0 the value of ω where this limit is reached. For $\omega>E_0$, the correlation function $C(\omega)\propto 1/\omega^2$ decreases down to zero. Such a behavior implies that two eigenfunctions separated by an energy difference $\omega>E_0$ try to *avoid each other*. That is, if a site $\mathbf{r}$ is occupied in one of the states it should be predominantly empty in the other.

To explain such a behavior, the following cartoon is useful. Let us define the *support* of an eigenfunction as the manifold of sites $\{\mathbf{r}\}$ where $|\Psi_i(\mathbf{r})|^2$ is essentially nonzero. To construct such a support starting from a given site $\mathbf{r}$ with the on-site energy $\varepsilon_{\mathbf{r}}$, we find all the sites in resonance with the site $\mathbf{r}$, i.e., such sites $\mathbf{r}'$ on which on-site energies $\varepsilon_{\mathbf{r}'}$ obey the relationship $|\varepsilon_{\mathbf{r}'}-\varepsilon_{\mathbf{r}}|<|H_{\mathbf{r},\mathbf{r}'}|$. Then the procedure should be repeated for all sites $\mathbf{r}'$ and so on. It is important that the so obtained manifold $\{\mathbf{r}\}$ does not always include all the sites of the system. If this is the case, the whole coordinate space is *stratified* into a set of mutually nonintersecting supports (Fig. 7).

Once the support is defined, one can build a *shell* of states on this support by making a linear combination of on-site states, pretty much in the same way as in building the conduction band states out of the on-site states in the tight-binding model. Then, by construction, the eigenfunctions belonging to the same shell are well overlapping, but those belonging to different shells do not overlap.

From this cartoon, it is clear that the physical meaning of the scale E_0 is the width of the energy band corresponding to a single shell. Indeed, if the energy separation ω greatly exceeds the typical single-shell bandwidth, the two eigenfunctions must belong to different shells and, thus, do not significantly overlap in space. On the contrary, if ω is smaller than

the single-shell bandwidth, the two states typically belong to the same shell and, thus, overlap strongly no matter how sparse the shell support.

The new energy scale E_0, which is the upper energy cutoff of the multifractal correlations, corresponds to a new length scale

$$\ell_0 = \frac{1}{(\rho E_0)^{1/d}}, \tag{18}$$

which has a meaning of the minimum length scale of the fractal texture. In the d-dimensional Anderson model, the energy scale E_0 can be estimated as

$$E_0 \sim V \sim D/W_c \sim D/2d \ln 2d,$$

where D is the total bandwidth. Estimating the DOS as $\rho = 1/a^3 D$, we find $\ell_0 \sim a W_c^{1/d}$, where a is the lattice constant.

Clearly, the picture with a stratified coordinate space is possible for PLBRM Eq. (3) with small enough $b < 1$ when the single-shell bandwidth $E_0 \sim b$ is small compared to the total bandwidth ~ 1. Amazingly, the 3D Anderson model, the low-frequency critical features of which are well described by the critical PLBRM with $b \approx 0.42$, also follows the predictions of the critical PLBRM for high frequencies $\omega > E_0$. This is a consequence of a relatively large value $W_c = 16.5$ of the critical disorder, which results in E_0 considerably smaller than the conduction bandwidth D. In particular, its coordinate space must be stratified to explain the observed (see Fig. 6) mutual avoidance of eigenstates.

VII. MULTIFRACTAL INSULATOR

As has been demonstrated in Sec. V, critical eigenfunctions with $\xi > L$ are strongly correlated in space. Here, we consider the case of the multifractal insulator, where the localization radius ξ is large compared to relevant microscopic lengths (the lattice constant or elastic scattering length) but is much smaller than the system size L. We will identify a suitable random-matrix model to describe this case and compare the properties of eigenfunction correlation in this model with those of the 3D Anderson model.

A. Ideal insulator limit

We start by considering a limit of strong disorder when the localization length $\xi \sim 1$ and the multifractal nature of eigenstates does not show up. A common wisdom is that in the strongly localized regime, the positions of the localization centers are completely uncorrelated. As it is shown in the Introduction, this leads to

$$NC(\omega) = 1, \tag{19}$$

which we will refer to as the *ideal insulator limit*. Figure 1 shows how this limit is reached in the ensemble of banded random matrices.

Note that $C(\omega)$ in this limit is much smaller than the self-overlap of $|\Psi(\mathbf{r})|^2$ given by the inverse participation ratio Eq. (4). Only for very small energy separations (typically $\propto e^{-L/\xi}$), which we will not be considering here, can the IPR limit be approached.

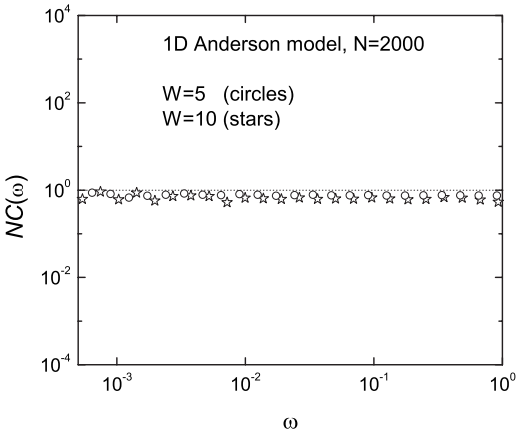

FIG. 8. Eigenfunction correlation in the 1D Anderson insulator with rectangular distribution of on-site energies and periodic boundary conditions. The disorder strengths are $W=5$ (circles) and $W=10$ (stars). The inverse participation ratios are equal to 0.23 and 0.46, respectively.

Now let us see how the correlation function $C(\omega)$ looks for the strong Anderson insulator. The corresponding plot for the 1D Anderson model is shown in Fig. 8. It coincides almost exactly with the ideal insulator limit Eq. (19).

The plot for the 3D Anderson model is shown in Fig. 9. One can see that $NC(\omega)$ is significantly enhanced at small energy separations and does not resemble at all the correlation function in the 1D Anderson insulator.

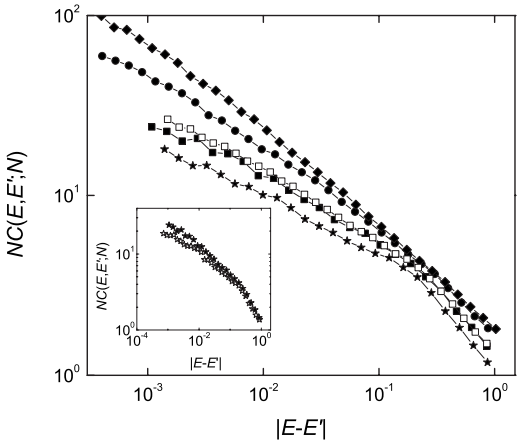

FIG. 9. Eigenfunction correlation in the 3D Anderson insulator with rectangular distribution of on-site energies and periodic boundary conditions. The disorder strengths are $W=80$ (stars), $W=60$ (squares), $W=40$ (circles), and $W=30$ (diamonds). The system size is $L=20$ for filled symbols and $L=8$ for open symbols. The inverse participation ratios for the four insulating systems are $P_2=0.72$, 0.63, 0.44, and 0.28, which correspond to $\xi=1.0$, 1.1, 1.2, and 1.4 according to $\xi=(9/4\pi P_2)^{1/3}$. The change of the slope occurs at $|E-E'|=\delta_\xi$. The slope for larger energy separations $|E-E'|>\delta_\xi$ progressively increases with increasing W, remaining smaller than 1. The inset shows the result for $W=60$, $L=20$ for the periodic (filled stars) and the hard wall (open stars) boundary conditions.

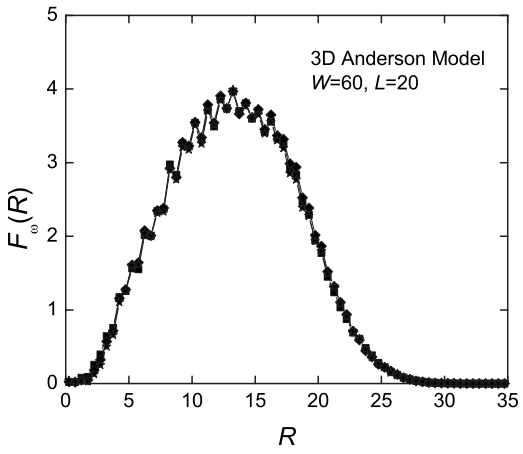

FIG. 10. The probability density Eq. (20) of having two centers of localization at a distance R in real space and at distances $\omega=0.011$ (squares), 0.0035 (diamonds), and 0.0015 (stars) in the energy space computed for the 3D Anderson model in the strong localization regime ($W=60$, $\xi=1.1$, and $L=20$). The repulsive core $R_0\sim 10-12$ exceeds the "hard ball" limit 2ξ by a factor of 5–6.

B. Repulsion of centers of localization for $R\gg\xi$

In order to understand why the ideal insulator limit is not reached in the 3D case despite the ratio $\xi/L>10$, we compute numerically the probability distribution function (PDF)

$$F_\omega(R)=\langle\delta(\omega-E_n+E_m)\delta(R-|\mathbf{r}_n-\mathbf{r}_m|)\rangle \tag{20}$$

of the distance $R=|\mathbf{r}_n-\mathbf{r}_m|$ between the points $\mathbf{r}_n$ and $\mathbf{r}_m$ in *real space* (*centers of localization*) where $|\Psi_{n,m}(\mathbf{r})|^2$ has an absolute maximum, provided that the energy separation between the states n,m is ω.

The results are shown in Fig. 10. It is seen that the function $F_\omega(R)$ is far from being independent of R (which would imply the lack of correlations between centers of localization). In fact, there is a *repulsion* of centers of localization at distances $R<R_0\sim 12$, which shows up in the decreasing probability density to find two centers of localization close to each other. Note that R_0 is almost ten times larger than the localization radius ξ estimated from the inverse participation ratio P_2.

An explanation for this repulsion between centers of localization $\mathbf{r_n}$ and $\mathbf{r_m}$ is based on the resonance interaction between states $\Psi_n(\mathbf{r})$ and $\Psi_m(\mathbf{r})$ if the energy distance between them is smaller than the typical overlap integral $V_{nm}(R)\propto e^{-R/2\xi}$.

The size of the repulsion core R_0 can be estimated from the equation

$$V_{nm}(R_0)=\omega,\quad \Rightarrow R_0\sim 2\xi\ln\left(\frac{\delta_\xi}{\omega}\right). \tag{21}$$

The characteristic energy scale δ_ξ is the mean level separation for states localized in the same volume ξ^d. Thus, the repulsion of centers of localization is a direct consequence of repulsion of energy levels for states confined in the same volume ξ^d. The energy scale δ_ξ depends on the strength of disorder and is of the order of the Fermi energy for strongly localized states. At $\omega\ll\delta_\xi$, the size of the repulsion core R_0 may considerably exceed the localization radius.

The qualitative picture of repulsion of centers of localization can be quantitatively confirmed using the analytical theory Eqs. (11)–(14) for the almost diagonal Gaussian RMT. To this end, we look at the contribution of $\bar{\omega}\gg 1$ to the sum in Eq. (12). Replacing the summation over n by integration, we obtain the contribution to $NC(\omega)$:

$$\int_{\sigma(n)<\omega}\frac{2\sigma^2(n)}{\omega^2}dn. \tag{22}$$

This equation can be easily interpreted using an elementary perturbation theory. Indeed, for strongly localized states $\Psi_m(\mathbf{r}_n)$, the eigenfunction correlation function can be represented as follows:

$$C_{nm}=\sum_{\mathbf{r}}|\Psi_n(\mathbf{r})|^2|\Psi_m(\mathbf{r})|^2\approx|\Psi_m(\mathbf{r_n})|^2\sum_{\mathbf{r}}|\Psi_n(\mathbf{r})|^2$$
$$+|\Psi_n(\mathbf{r_m})|^2\sum_{\mathbf{r}}|\Psi_m(\mathbf{r})|^2\approx|\Psi_m(\mathbf{r_n})|^2+|\Psi_n(\mathbf{r_m})|^2. \tag{23}$$

The amplitude at the tail of the wave function $|\Psi_n(\mathbf{r_m})|^2$ with the maximum at a point $\mathbf{r}_n$ can be computed from the elementary perturbation theory, in which the wave function of the zeroth approximation corresponding to the energy ε_n is $|\Psi_n^{(0)}(\mathbf{r})|^2=\delta_{\mathbf{r},\mathbf{r}_n}$:

$$|\Psi_n(\mathbf{r_m})|^2=|\Psi_m(\mathbf{r_n})|^2\approx\frac{|H_{nm}|^2}{(\varepsilon_n-\varepsilon_m)^2}\approx\frac{|H_{nm}|^2}{\omega^2}\ll 1. \tag{24}$$

The fluctuating *on-site* energy ε_n is the main part of the eigenvalue E_n for a sufficiently strongly localized state. Thus, we come to a conclusion that the amplitude of the wave function Ψ_n at a center of localization of the wave function Ψ_m is inversely proportional to $(E_n-E_m)^2=\omega^2$ and, thus, is strongly *enhanced* when $\omega\ll\delta_\xi$. At a first glance, this is in contradiction with the common wisdom that $|\Psi_n(\mathbf{r}_m)|^2\propto e^{|\mathbf{r}_n-\mathbf{r}_m|/\xi}$, which is apparently ω independent. The point is that the quantity $|\Psi_n(\mathbf{r})|^2$ has many accidental spikes due to resonances between on-site energies. The measure of such resonance points is small and, for some (but not all) purposes, one can neglect them and approximate $|\Psi_n(\mathbf{r})|^2\propto e^{|\mathbf{r}_n-\mathbf{r}_m|/\xi}$. The best known example when the two-spike eigenfunction makes the main contribution is the low-frequency conductivity in the localized phase.[28] As we will see below, here we deal with a very similar phenomenon.

Now the correlation function $C(\omega)$ can be computed just by averaging over disorder and the distance $\mathbf{R}=\mathbf{r}_n-\mathbf{r}_m$:

$$C(\omega)=\int F_\omega(R)\langle C_{nm}(R)\rangle d^dR\approx\int F_\omega(R)\frac{2\langle|H_{nm}|^2\rangle}{\omega^2}d^dR, \tag{25}$$

where $F_\omega(R)$ is the PDF defined by Eq. (20).

Comparing Eq. (25) for $d=1$ with Eq. (22), we see that

$$F_\omega(R) = 1/N \quad (R \gg R_0), \tag{26}$$

where R_0 is found from the condition $\sigma(R_0)=\omega$ similar to Eq. (21).

In the opposite limit $R \ll R_0$, or $\omega \ll \sigma(R)$, we have a resonance enhancement $|\Psi_m(\mathbf{r}_n)|^2 \approx 1/2$ and $C_{nm} \approx 1$. Then the comparison of Eq. (25) with Eq. (12) yields

$$F_\omega(R) = \frac{4}{3N}\left(\frac{\omega}{\sigma(R)}\right)^2 \quad (R \ll R_0). \tag{27}$$

C. Logarithmic enhancement of correlations of localized eigenfunctions and the truncated critical random-matrix theory

Now let us consider Eq. (25) for $d \geqslant 1$ assuming that all states are exponentially localized and, thus, $\langle |H_{nm}|^2 \rangle \propto \exp[-R/\xi]$. We also assume for simplicity that $F_\omega(R) = N^{-1}\theta(R-R_0)$, where $R_0 = 2\xi \ln(\delta_\xi/\omega)$. Then one immediately obtains from Eq. (25) that, due to the phase volume factor R^{d-1}, the correlation of exponentially localized eigenfunctions depends crucially on the dimensionality of space. Namely, for $d=1$, the ideal insulator limit Eq. (19) is reached for sufficiently small ξ (see Fig. 1), while for $d>1$ and $\omega \ll \delta_\xi$, the correlation function acquires a logarithmic in ω enhancement factor:

$$NC(\omega) \sim \xi^{d-d_2} \ln^{d-1}\left(\frac{\delta_\xi}{\omega}\right). \tag{28}$$

The physics behind this result is similar to the one which leads to the celebrated Mott law,[28–30] $\sigma(\omega) \propto \omega^2 \ln^{d+1}(\delta_\xi/\omega)$ for the ac conductivity $\sigma(\omega)$ at $\omega \ll \delta_\xi$. The difference is that the contribution to conductivity from the resonance states with the distance R between the points of maximal amplitude is proportional to the square of the dipole moment $d^2 \propto R^2$, so that the phase volume factor R^{d-1} gets multiplied by R^2, resulting in the emergence of the logarithmic factor $\ln^{d+1}(\delta_\xi/\omega)$ instead of $\ln^{d-1}(\delta_\xi/\omega)$ in our case.[30]

Below we obtain this result for the *truncated critical* RMT defined by Eq. (8). The phase volume factor R^{d-1} can be formally taken into account in the random-matrix formalism Eq. (12) if one assumes the following relationship between the d-dimensional vector $\mathbf{R}$ and the difference of matrix indices $n-m$:

$$d(n-m) \Rightarrow \Omega_d R^{d-1} dR, \quad |n-m| \Rightarrow \frac{\Omega_d}{d} R^d, \tag{29}$$

where Ω_d is the total solid angle in the d-dimensional space.

In particular, Eq. (29) suggests that for exponential localization, the correct truncating factor in Eq. (8) has the form

$$e^{-R/\xi} \Rightarrow \exp\left[-\left(\frac{|n-m|}{B}\right)^{1/d}\right]. \tag{30}$$

This sets the exponent η in Eq. (8) equal to

$$\eta = \frac{1}{d}. \tag{31}$$

Then Eq. (12) can be used, which is convenient to rewrite in the following form:

$$NC(\omega) \approx k(\omega) = -\int_0^\infty f(y) \frac{dy}{\left.\frac{d}{dn}[\ln \sigma^2(n)]\right|_{n=n(y)}}, \tag{32}$$

where $n(y)$ is found from the equation

$$y = \frac{\omega^2}{2\sigma^2[n(y)]}$$

and

$$f(y) = \left(\frac{2}{\sqrt{y}} + \frac{1}{y\sqrt{y}}\right)e^{-y}\int_0^{\sqrt{y}} e^{t^2} dt - \frac{1}{y} = \begin{cases} \dfrac{4}{3}, & y \ll 1 \\ \dfrac{1}{y^2}, & y \gg 1. \end{cases} \tag{33}$$

For the truncated critical RMT Eq. (8) with $\eta = 1/d$, one finds

$$-\frac{1}{\frac{d}{dn}[\ln \sigma^2(n)]} = \frac{n}{2 + \frac{1}{d}\left(\frac{n}{B}\right)^{1/d}},$$

where

$$n(y) = \begin{cases} B \ln^d\left(\dfrac{2b^2 y}{\omega^2 B^2}\right), & \dfrac{\omega}{\sqrt{y}} \ll \delta_\xi \sim \dfrac{b}{B} \\ \sqrt{\dfrac{2b^2 y}{\omega^2}}, & \dfrac{\omega}{\sqrt{y}} \gg \delta_\xi. \end{cases} \tag{34}$$

The integral in Eq. (32) is well convergent and, thus, mainly contributed by $y \sim 1$. This makes it possible to obtain a simple analytical expression for $NC(\omega)$:

$$NC(\omega) \approx \begin{cases} c_d B \ln^{d-1}\left(\dfrac{\delta_\xi}{\omega}\right), & \omega \ll \delta_\xi \sim b/B \\ c_0\left(\dfrac{b}{\omega}\right), & E_0 \sim b \gg \omega \gg \delta_\xi, \end{cases} \tag{35}$$

where

$$c_d = 2^{d-1} d \int_0^\infty f(y) dy = 2^d d,$$

$$c_0 = \int_0^\infty f(y) \sqrt{\frac{y}{2}} dy = \left(\frac{\pi}{2}\right)^{3/2} \approx 1.97.$$

The first line of Eq. (35) is consistent with Eq. (28), in which $d_2/d \sim b \ll 1$ and $\xi \sim B^{1/d}$. The power-law behavior in the second line of Eq. (35) is a remnant of the critical behavior Eq. (6). It exists only for considerably large $B \gg 1$, where $\delta_\xi \ll E_0 = c_0 b$, i.e., only in the multifractal insulator. For a very strong insulator with $\delta_\xi \gg E_0$, the localization radius is smaller than the minimal length scale ℓ_0 of the fractal texture. This is the region of an ordinary insulator where the entire localization volume is more or less homogeneously filled.

Thus, the eigenfunction correlation function for the truncated critical RMT Eq. (8) interpolates between the behavior given by Eq. (28) at $\omega \ll \delta_\xi$ [or $L_\omega=(\rho\omega)^{-1/d} \gg \xi$] and the critical behavior Eq. (6) which is valid for $\ell_0 \ll L_\omega \ll \xi$. At $L_\omega \sim \xi$, both asymptotic forms apparently match each other.

The physical picture that leads to such a behavior is the following. There are two distinct regions $L_\omega < \xi$ and $L_\omega > \xi$ where the physics of eigenfunction correlations is entirely different. In the case $L_\omega < \xi$, the characteristic length L_ω has a meaning of the period of beating in the overlap of two fractal eigenfunctions inside the localization volume. The regions where two fractal supports match each other well alternate with the regions with a strong mismatch between them, very much like in the case of two grids with slightly different periods. The regions of strong overlap make the main contribution

$$C_m \sim P_2 \sim (L_\omega/\ell_0)^{d-d_2}/\xi^d$$

to the eigenfunction correlation function $C(\omega)$, which is of the order of the IPR of a multifractal metal (see next section for more details), with the system size equal to the localization radius ξ and the correlation length equal to the size L_ω of the well overlapping regions. To obtain the correlation function $C(\omega)$, one has to multiply $C_m(\omega)$ by the probability for the entire localization volumes to overlap. This probability is ξ^d/L^d, as for $\omega > \delta_\xi$ there is no correlation in the positions of the localization volumes. Thus, we obtain the critical power law Eq. (6): $NC(\omega) \sim (L_\omega/\ell_0)^{d-d_2} = (E_0/\omega)^{1-d_2/d}$.

For $L_\omega > \xi$, the physics of eigenfunction correlations changes drastically. Now localization volumes statistically repel each other and the overlap is only due to the tails. In this region, the length scale L_ω loses its physical meaning, which is taken over by the length scale R_0 given by Eq. (21).

The overall shape of $C(\omega)$ with the logarithmic enhancement factor $\ln^{d-1}(\delta_\xi/\omega)$ obtained within the truncated critical RMT describes the numerical results on the 3D Anderson model very well (see Fig. 11). The absence of this factor at $d=1$ explains the qualitative difference between the case $d=1$ (see Fig. 8) and $d=3$ (see Fig. 9). This difference is essentially due to a competition between two effects: (i) repulsion of centers of localization and (ii) resonance enhancement of overlap by tails. The first effect tends to decrease the probability of the overlap of localization volumes. The second effect increases the eigenfunction overlap by means of tails. In the 1D case, these two effects compensate each other, and the result is the same as one would obtain for completely uncorrelated positions of localization volumes and the typical exponentially decreasing tails. In higher dimensions, the enhancement of overlap in the tail region prevails because of the increased volume of those regions.

Concluding this section, we claim that the truncated critical RMT provides an excellent description of the 3D Anderson insulator both in the strong localization region (see Fig. 9) and in the region of the multifractal insulator, where the localization radius is large and the corresponding scale δ_ξ is small compared with the upper cutoff E_0 of the multifractal correlations. Because of the limited size of the 3D lattice, this latter region is out of reach for numerical simulations on the 3D Anderson model, and the random-matrix theory is the only mathematical model which properly describes the physics of the multifractal insulator.

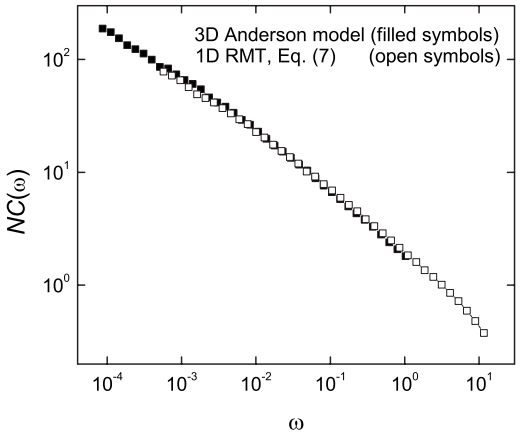

FIG. 11. A comparison of eigenfunction correlation functions for the 3D Anderson model with $W=30$ and $L=20$, and the truncated critical RMT Eq. (7) with $b=0.42$, $B=5$, $\eta=1/3$, and $N=2000$. The IPR takes values of $P_2=0.28$ and 0.25, respectively. The scale of $\omega=|E-E'|$ is different in those two cases by approximately a factor of 11.

D. Supercritical power-law banded random matrix

Note that there is another RMT Eq. (9) suggested in Ref. 14 as a candidate to describe eigenfunction correlations in the multifractal insulator. Below we show that this *supercritical* PLBRM is principally flawed, as it corresponds to a power-law localization which is not the case in the 3D Anderson model.

This can be best demonstrated by Eq. (24), in which $|H_{nm}| \Rightarrow \sigma(R)=(b/R)^\alpha$ with $\alpha > 1$. Accordingly, the typical scale for the repulsion of centers of localization is

$$R_\omega = \frac{b}{\omega^{1/\alpha}}. \tag{36}$$

In Fig. 12, we plot the results of numerical calculation of the PDF $F_\omega(R)$ for the supercritical PLBRM Eq. (9). The characteristic scale R_ω where $F_\omega(R)$ reaches its maximum is seen well in this plot.

The analytical treatment based on Eq. (32) yields for this model

$$NC(\omega) = \left(\frac{E_\alpha}{\omega}\right)^{1/\alpha} \sim R_\omega, \tag{37}$$

where $E_\alpha=(c_\alpha b)^\alpha$ and

$$c_\alpha = \frac{\pi^{3/2}}{2^{[1+(1/2\alpha)]}} \frac{1}{\Gamma\left(\frac{3}{2}-\frac{1}{2\alpha}\right)}.$$

Similar to the entire approach based on Eq. (12), the above results are valid when b is the smallest relevant parameter. In the problem of PLBRM with α close to 1, there is a compe-

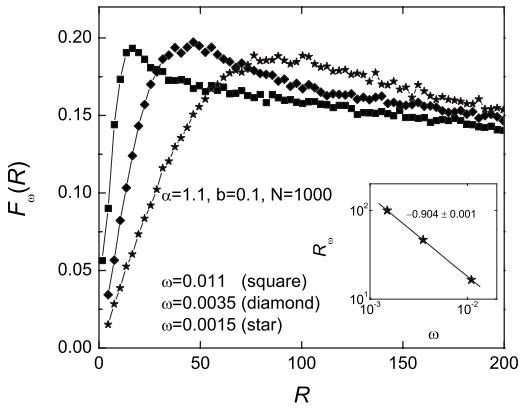

FIG. 12. The correlation function of centers of localization $F_\omega(R)$ for the supercritical PLBRM Eq. (9) with $\alpha=1.1$, $b=0.1$, and $N=1000$ for $\omega=0.011$ (squares), 0.0035 (diamonds), and 0.0015 (stars). The inset shows the ω dependence of R_ω, where $F_\omega(R)$ reaches its maximum. The finite slope of $F_\omega(R)$ for $R \gg R_\omega$ is a finite-size effect, which was neglected in Eq. (26).

tition between the small parameters $|1-\alpha|$ and b, so that the validity of Eqs. (36) and (37) requires also $\alpha-1 \gg b$.

We see that in the infinite system $N\to\infty$, the power law Eq. (37) in $C(\omega)$ is not restricted at small ω, and no energy scale similar to δ_ξ emerges. This can be explained only if we assume that the localization length for $\alpha-1 \gg b$ is of order 1. Then for all energy separations $\omega \gg E_\alpha$, the repulsion core $R_\omega \gg \xi$ and no qualitative change in the correlation function occurs until R_ω hits the system size N. For smaller ω, the correlation function is almost a constant. This quantitative analysis is illustrated by Fig. 13.

The region of α that could describe the multifractal insulator with large $\xi \gg 1$ corresponds to $\alpha-1 \ll b$. In this case, an energy scale similar to δ_ξ should appear. It can be found from the condition

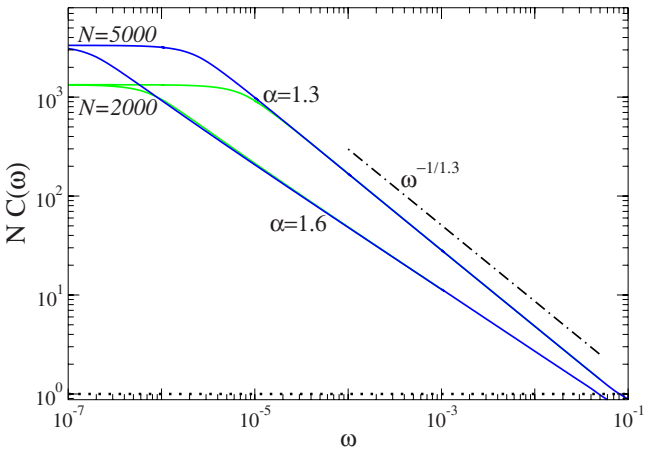

FIG. 13. (Color online) Two-eigenfunction correlation for the supercritical PLBRM Eq. (9) with $\alpha-1 \gg b$ calculated analytically using Eqs. (11)–(14). The power law $C(\omega) \propto \omega^{-1/\alpha}$ is valid for all energy separations corresponding to $1<R_\omega<N$. The onset of the plateau moves to $\omega\to 0$ in the limit $N\to\infty$. The ideal insulator limit is reached by decreasing the slope with increasing α.

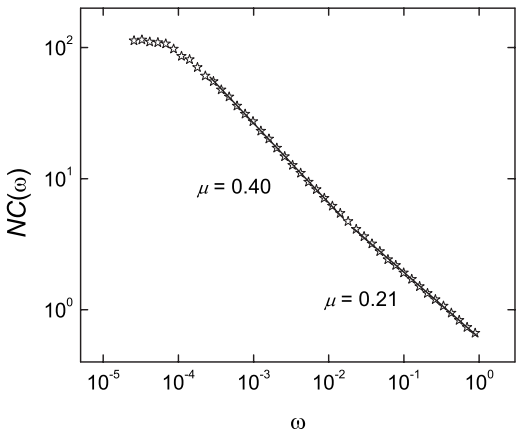

FIG. 14. Two-eigenfunction correlation for the supercritical PLBRM Eq. (9). Numerical results for $\alpha-1<b$ (this plot corresponds to $\alpha=1.15$, $b=0.45$, and $N=5000$) show that the exponent μ of the power law $C(\omega) \propto \omega^{-\mu}$ changes at $|E-E'|=\delta_\xi$, with the larger value corresponding to smaller energy separations.

$$R_\omega|_{\omega=\delta_\xi} = \xi(\alpha), \quad \Rightarrow \delta_\xi \approx \frac{E_0}{\xi}. \tag{38}$$

At $|E-E'|=\delta_\xi$, the slope on the log-log plot of $C(\omega)$ should change from the critical value at $\delta_\xi<|E-E'|<E_0$ to a different (but constant) α-dependent value at $|E-E'|<\delta_\xi$. This change of the slope is clearly seen in the numerical simulations on the supercritical PLBRM presented in Fig. 14. It appears that in all cases studied, the slope μ at $|E-E'|<\delta_\xi$ is *larger* than that at $|E-E'|>\delta_\xi$. This is in clear contradiction to the results (see Fig. 9) obtained in the 3D Anderson insulator.

An important conclusion we can draw from the above analysis of the supercritical PLBRM is that the correlation function $C(\omega)$ for $\omega<\delta_\xi$ is the power law in this model. This can be traced back to the power-law character of localization in the supercritical PLBRM, which is not the case in the disordered lattice models (such as the 3D Anderson model) with short-range hopping integrals. This is the reason why the supercritical PLBRM is not suitable for describing the insulating phase of the 3D Anderson model.

VIII. SEARCH FOR RANDOM-MATRIX MODEL FOR A MULTIFRACTAL METAL

A. Antitruncated critical random-matrix theory

Surprisingly, the natural counterpart to the truncated critical RMT Eq. (8), which is defined by Eq. (10) ("antitruncated" critical RMT), does not describe extended states in the multifractal metal. The reason is that this model possesses two low-frequency system-size independent energy scales instead of the single scale δ_ξ, which is associated with the size ξ of a multifractal cell in Fig. 2(c). In order to see this, we analyze the analytical formulas Eqs. (11)–(14) with the variance defined by Eq. (10).

To this end, we expand the summand of Eq. (12) in $1/\bar{\omega} \ll 1$ to arrive at the formula similar to Eq. (22), but with

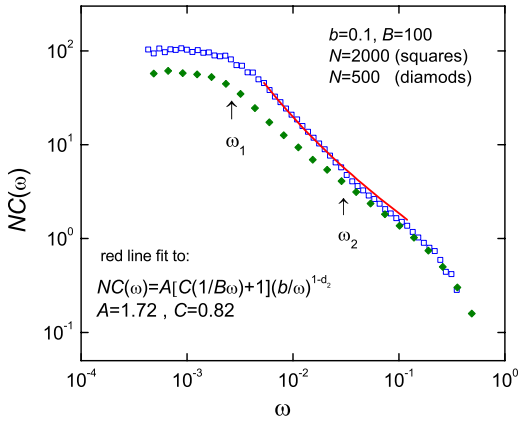

FIG. 15. (Color online) Numerics on the antitruncated critical RMT of the orthogonal symmetry class. The predicted analytically nonmonotonous behavior of log-log slope controlled by the energy scale ω_2 is well seen both for small and large system sizes. The solid line is a fit according to Eq. (40).

the upper limit of integration equal to the correlation radius ξ:

$$NC(\omega) = \frac{2}{\omega^2}\int_{\sigma(n)<\omega}^{\xi} \sigma^2(n)dn, \tag{39}$$

where $\xi = B/2b$ according to Eq. (16).

Substituting Eq. (10) for $\sigma(n)$, we arrive at

$$NC(\omega) = \frac{b^2}{\omega^2}\int_{b/\omega}^{\xi}\left[\frac{1}{n^2}+\frac{2}{B^2}\right]dn \approx \frac{b}{\omega}+2\xi\frac{b^2}{\omega^2 B^2}. \tag{40}$$

Equation (40) is valid at $\omega > b/\xi$ when the upper limit of integration is larger than the lower limit. This sets the energy scale $\omega_1 = b/\xi = 2b^2/B$.

Another scale $\omega_2 = 1/2b\xi$ gives the crossover scale that separates the critical $1/\omega$ behavior and the $1/\omega^2$ behavior that takes place for intermediate frequencies $\omega_1 < \omega < \omega_2$. While the scale $\omega_1 = b/\xi$ (similar to the scale $\delta_\xi = b/B$ in a 1D insulator) determines the onset of the low-frequency plateau, the second relevant scale ω_2 that appears in the model Eq. (10) seems to have no physical meaning. Indeed, the existence of this scale leads to a characteristic form of the correlator $C(\omega)$, the log-log plot of which has a significant slope increase just before it drops to zero at the plateau (see Figs. 15 and 16).

We did not find a behavior of such type in the 3D Anderson metal (see Fig. 17). The plot in Fig. 17 clearly shows a saturation[31] at $\omega < \omega_1$:

$$C(\omega) \approx \frac{1}{3}P_2 = A_m\frac{\xi^{d-d_2}}{3L^d}, \quad A_m \approx 0.5. \tag{41}$$

However, there is no evidence of a maximum in the slope just above the onset of the plateau.

B. Subcritical power-law banded random matrix

Now we consider the subcritical PLBRM ensemble defined by Eq. (9) with $1/2 < \alpha < 1$. In this case, analytical

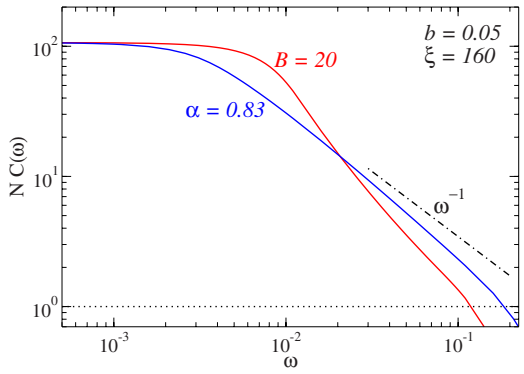

FIG. 16. (Color online) Eigenfunction correlation for the antitruncated critical RMT Eq. (8) (labeled by $B=20$) and for the subcritical PLBRM Eq. (9) (labeled by $\alpha=0.83$) of unitary symmetry class computed analytically from Eqs. (11)–(14). For the antitruncated critical RMT, the nonmonotonous behavior of log-log slope is similar to the one in Fig. 15.

arguments similar to Eqs. (39) and (40) predict only one relevant energy scale $\omega_1 = b/\xi^\alpha$, such that for $\omega < \omega_1$, the correlation function $C(\omega)$ is constant and, for $\omega > \omega_1$ (but $\omega < E_0 \sim b^\alpha$), it is a pure power law $C(\omega) \propto \omega^{-1/\alpha}$. Thus, the subcritical PLBRM is free from the drawback related to the unphysical second energy scale. For comparison, we plotted in Fig. 16 the analytical results for the antitruncated critical RMT and for the subcritical PLBRM. It is seen that the overall shape of the PLBRM curve for subcritical PLBRM is much closer to the results of the 3D Anderson model of Fig. 17.

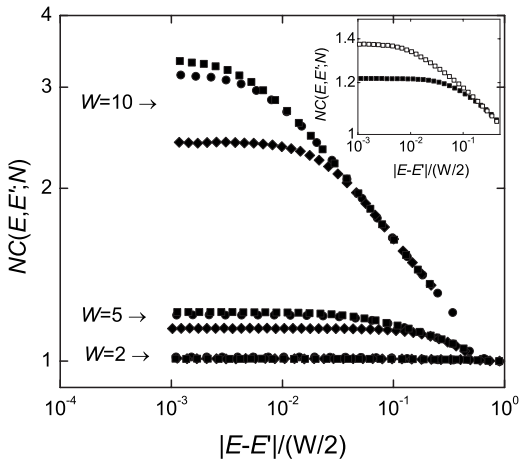

FIG. 17. Eigenfunction correlation in the 3D Anderson model: extended states. The disorder strengths are $W=2$, $W=5$, and $W=10$ as indicated by arrows. The system sizes are $L=8$ (diamonds), $L=16$ (circles), and $L=20$ (squares). The correlation length is estimated from the inverse participation ratio as follows: $\xi = (P_2 N/A_m)^{1/(d-d_2)}$ ($A_m=0.5, d_2=1.3$), and is equal to $\xi=5.8$, 3.2, and 2.8 at $W=10$, 5, and 2, respectively. In the inset, we compare results for $W=5$ and $L=20$ for the periodic (filled squares) and the hard-wall (open squares) boundary conditions. For hard-wall boundary conditions, the correlation function looks "more critical" as the critical point $W_c=15.2$ in this case is closer to $W=5$.

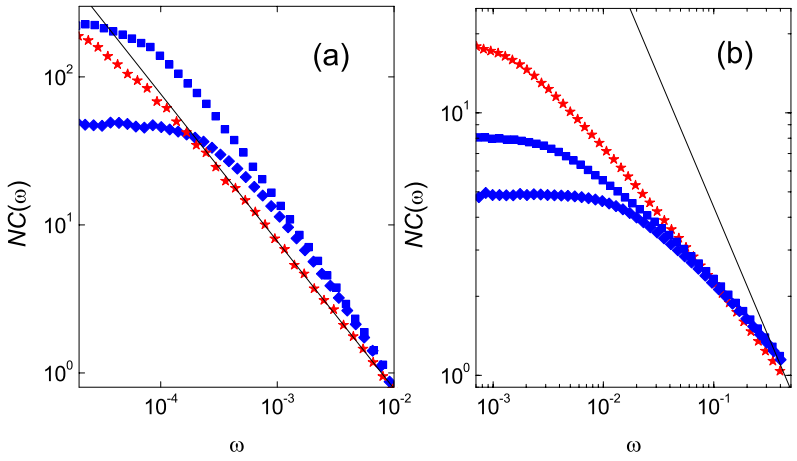

FIG. 18. (Color online) Eigenfunction correlations in the subcritical PLBRM of the orthogonal symmetry class. (a) The small-b limit: $b=0.001$, $\alpha=0.8$ at $N=1000$ (squares) and $N=200$ (diamonds). The critical correlations for $b=0.001$, $\alpha=1$, and $N=1000$ are shown by stars. The solid line corresponds to the power law ω^{-1}. The slope of the subcritical curve is larger than 1 (correlations are short range in the energy space). This case is relevant for the metallic phase of the Anderson model in very high dimensions. (b) The case $b=0.4$, $\alpha=0.95$ at $N=1000$ (squares) and $N=200$ (diamonds) is relevant for the Anderson model in $d=3$ (multifractal metal). The slope is less than the critical (which, in turn, is less than 1) and is almost size independent. Correlations are long range in the energy space.

Note, however, that the power law emerging in the analytical results for the subcritical PLBRM has an exponent $1/\alpha$ which is larger than the critical exponent. Computer simulations [see Fig. 18(a)] on the subcritical PLBRM with very small b confirm this analytical result as $N\to\infty$ extrapolation and show that the slope increases with increasing system size N. However, the slope of the corresponding curves for the 3D Anderson model of Fig. 17 is almost independent of the system size and is equal to or *smaller* than the critical slope.

The reason for the discrepancy is that the analytical result for the slope $\mu=1/\alpha$ corresponds to the limit $b\to 0$. At a finite b, the slope decreases with increasing b and, at a sufficiently large b, may become smaller than the critical one. It is reasonable to assume that at small $1-\alpha$ and b, this happens at $b\sim 1-\alpha$. The relevance of the parameter $b/(1-\alpha)$ is also seen from the expression for the correlation length ξ

$$\xi \sim \exp\left[\frac{a_\alpha}{1-\alpha}\right], \quad a_\alpha = \ln\left(\frac{1-\alpha}{b^\alpha}\right) + \text{const}, \qquad (42)$$

which was found (up to a constant of order 1) analytically from Eq. (16). This expression is apparently meaningless for $b^\alpha \gg 1-\alpha$, where c_α may become negative.

Numerical simulations on the subcritical PLBRM with $1-\alpha<b$ (e.g., for $\alpha=0.95$ and $b=0.4$ relevant for the 3D Anderson model) show [see Fig. 18(b)] that the log-log slope of $C(\omega)$ is somewhat smaller than the critical one and is almost independent of the matrix size N. Thus the subcritical PLBRM shows exactly the same character of eigenfunction correlations as in the 3D Anderson metal (see Fig. 17).

Two parameters of the subcritical PLBRM allow us to simulate the effect of the finite correlation length (choice of $\alpha<1$) and the dimensionality of space (choice of b). Note in this connection that for the disorder strength W significantly smaller than the critical value W_c, not only α but also b is W dependent. The point is that in the 3D Anderson model, the variance of the on-site energy fluctuations is proportional to W^2, while the off-diagonal hopping integral is equal to 1. This implies that the ratio of a typical off-diagonal to a typical diagonal element controlled in Eq. (9) by the parameter b should scale like $1/W$. As the log-log slope of $C(\omega)$ decreases with increasing b, moving away from the Anderson transition into the *metallic* phase $W<W_c$ has an effect of *decreasing* the slope. On the insulator side of the transition, the situation is opposite and one should expect an *increase* of the slope (for $\delta_\xi<\omega<E_0$) with increasing W. Figure 9 shows that it is apparently the case.

Another relevant note is that for the Anderson model in *higher dimensions*, the correlation dimension d_2 decreases. This can be modeled by a decreasing parameter b. Then the analogy with the subcritical PLBRM suggests that for sufficiently high dimensions $d>d_c$, the behavior in the d-dimensional Anderson model should become similar to the one in Fig. 18(a). Namely, the exponent μ in Eq. (7) may become *larger than* 1. This changes qualitatively the eigenfunction correlations, as they become effectively short range in the energy space. In particular, the return probability,[9] which is proportional to the Fourier transform of $C(\omega)$, behaves in the time interval $\hbar/E_0 \ll t \ll \hbar/\delta_\xi$ as $P(t)\propto t^{-(1-\mu)}$ for $\mu<1$, and is a constant for $\mu>1$.

We believe that this qualitative change in the eigenfunction statistics (if confirmed for a d-dimensional Anderson model with $d>d_c$) should lead to dramatic physical consequences, marking a transition to a different metallic state.

IX. CONCLUSION

In conclusion, we list the main results obtained above. The most important of them is the persistence—beyond the point of localization transition—of the critical power law in the dependence of the eigenfunction correlation function

$C(\omega)$ on the energy separation ω and the related enhancement of $C(\omega)$ at $\delta_\xi \ll \omega \ll E_0$, where δ_ξ is the mean level spacing in the localization and/or correlation volume, and E_0 is the upper energy cutoff of multifractality. This enhancement leads to an enhancement of matrix elements of local electron interaction, which may result in, e.g., an enhancement of the superconducting transition temperature in the vicinity of the Anderson localization transition.[18] Another important observation is that the enhancement of correlations at $\omega < E_0$ is always accompanied by the depression at $\omega > E_0$, both phenomena being the consequences of the stratification of the coordinate space into mutually avoiding supports of the fractal structure with well overlapping eigenfunctions living on each of them. An independent, but also important, phenomenon is the logarithmic enhancement of $C(\omega)$ in the 2D and 3D Anderson insulators at $\omega < \delta_\xi$ (and the absence of such enhancement in the quasi-1D disordered wire). It is a result of a competition of two simultaneous phenomena: the repulsion of centers of localization and the resonance enhancement of the eigenfunction overlap by tails. Both phenomena are studied quantitatively within the truncated critical random-matrix model Eq. (8), which is suggested in this paper as a universal tool to describe the localized eigenfunctions with a multifractal texture. It is constructed in such a way as to correctly describe also Mott physics of strongly localized eigenstates. We also show that (unlike its supercritical counterpart which is not suitable for describing an Anderson insulator) the subcritical power-law banded random-matrix ensemble Eq. (9) suggested in Ref. 14 describes the multifractal metal reasonably well. From the analytical solution for this RMT, we conclude that a critical dimensionality d_c may exist above which the d-dimensional Anderson model has an unusual metal phase characterized by an effectively short-range correlation function $C(\omega) \propto \omega^{-\mu}$ with $\mu > 1$.

ACKNOWLEDGMENTS

The authors are grateful to B. L. Altshuler, J. T. Chalker, M. V. Feigel'man, Y. V. Fyodorov, I. V. Lerner, A. Silva, and V. I. Yudson for stimulating discussions, and especially to O. Yevtushenko for collaboration at an earlier stage of this work and for help in preparing figures. E.C. thanks the FEDER and the Spanish DGI for financial support through Project No. FIS2004-03117.

[1] A. D. Mirlin, Phys. Rep. **326**, 259 (2000).
[2] I. L. Aleiner, P. W. Brouwer, and L. I. Glazman, Phys. Rep. **358**, 309 (2002).
[3] V. E. Kravtsov and A. D. Mirlin, JETP Lett. **60**, 656 (1994).
[4] A. D. Mirlin and Y. V. Fyodorov, JETP Lett. **60**, 790 (1994).
[5] M. L. Mehta, *Random Matrices* (Academic, San Diego, 1991).
[6] K. B. Efetov, *Supersymmetry in Disorder and Chaos* (Cambridge University Press, Cambridge, England, 1997).
[7] Y. V. Fyodorov and A. D. Mirlin, Phys. Rev. Lett. **67**, 2405 (1991).
[8] V. E. Kravtsov and K. A. Muttalib, Phys. Rev. Lett. **79**, 1913 (1997).
[9] J. T. Chalker, V. E. Kravtsov, and I. V. Lerner, JETP Lett. **64**, 386 (1996).
[10] V. I. Falko and K. B. Efetov, Europhys. Lett. **32**, 627 (1995).
[11] F. Wegner, Z. Phys. B **36**, 209 (1980).
[12] J. T. Chalker, Physica A **167**, 253 (1990).
[13] J. T. Chalker and G. J. Daniell, Phys. Rev. Lett. **61**, 593 (1988).
[14] A. D. Mirlin, Y. V. Fyodorov, F. M. Dittes, J. Quezada, and T. H. Seligman, Phys. Rev. E **54**, 3221 (1996).
[15] B. L. Altshuler, A. G. Aronov, and P. A. Lee, Phys. Rev. Lett. **44**, 1288 (1980).
[16] S. Maekawa and H. Fukuyama, J. Phys. Soc. Jpn. **51**, 1380 (1982); A. M. Finkelshtein, JETP Lett. **45**, 46 (1987).
[17] L. P. Gorkov, A. I. Larkin, and D. E. Khmelnitskii, JETP Lett. **30**, 228 (1979).
[18] M. V. Feigel'man, L. B. Ioffe, V. E. Kravtsov, and E. A. Yuzbashyan, Phys. Rev. Lett. **98**, 027001 (2007).
[19] T. Ohtsuki, K. Slevin, and T. Kavarabayashi, Ann. Phys. **8**, 655 (1999).
[20] A. Mildenberger, F. Evers, and A. D. Mirlin, Phys. Rev. B **66**, 033109 (2002); A. M. García-García and E. Cuevas, *ibid.* **75**, 174203 (2007).
[21] A. D. Mirlin and F. Evers, Phys. Rev. B **62**, 7920 (2000).
[22] T. Brandes, B. Huckestein, and L. Schweitzer, Ann. Phys. **5**, 633 (1996).
[23] L. Schweitzer and H. Potempa, Physica A **266**, 486 (1999).
[24] Y. V. Fyodorov and A. D. Mirlin, Phys. Rev. B **55**, R16001 (1997).
[25] O. Yevtushenko and V. E. Kravtsov, J. Phys. A **36**, 8265 (2003); O. Yevtushenko and V. E. Kravtsov, Phys. Rev. E **69**, 026104 (2004); V. E. Kravtsov, O. Yevtushenko, and E. Cuevas, J. Phys. A **39**, 2021 (2006).
[26] L. S. Levitov, Phys. Rev. Lett. **64**, 547 (1990).
[27] O. Yevtushenko and A. Ossipov, J. Phys. A: Math. Theor. **40**, 4691 (2007).
[28] N. F. Mott and E. A. Davis, *Electronic Properties in Non-crystalline Materials* (Clarendon, Oxford, 1971), Sec. 2.4.
[29] V. L. Berezinsky, Sov. Phys. JETP **38**, 620 (1974).
[30] A. Houghton, L. Schafer, and F. J. Wegner, Phys. Rev. B **22**, 3598 (1980).
[31] The constant A_m (and the corresponding constant A_i) for an insulator was found from an independent numerical study of an exponential tail $|\Psi(r)|^2 - |\Psi(\infty)|^2 \propto e^{-r/\xi}$ of the wave function, with r counted from the maximum of the wave function amplitude.